Experimental investigations and design provisions of steel-to-timber joints with annular-ringed shank nails for Cross-Laminated Timber structures

Matteo Izzi[1,2,], Georg Flatscher[3], Massimo Fragiacomo[4], Gerhard Schickhofer[5]*

[1] Ph.D. Candidate, Department of Engineering and Architecture, University of Trieste, Piazzale Europa 1, 34127 Trieste, Italy.

[2] Research Assistant, National Research Council of Italy - Trees and Timber Institute (CNR IVALSA), Via Biasi 75, 38010 San Michele all'Adige, Italy.

[3] Research and Teaching Associate, Institute of Timber Engineering and Wood Technology, Graz University of Technology, Inffeldgasse 24/1, 8010 Graz, Austria.

[4] Professor, Deputy Head, Department of Civil, Construction-Architectural and Environmental Engineering, University of L'Aquila, Via Gronchi 18, 67100 L'Aquila, Italy.

[5] Professor, Head, Institute of Timber Engineering and Wood Technology, Graz University of Technology, Inffeldgasse 24/1, 8010 Graz, Austria.

ABSTRACT

This paper investigates the mechanical and the hysteretic behaviour of steel-to-timber joints with annular-ringed shank nails in Cross-Laminated Timber (CLT). These fasteners are used to anchor typical metal connectors, such as hold-downs and angle brackets, to the CLT panels. The experimental programme presented in the paper was carried out at the Institute of Timber Engineering and Wood Technology, Graz University of Technology (Graz, Austria). Average and characteristic values of the experimental strength capacities are evaluated and compared to the analytical predictions determined according to current structural design codes and literature. Furthermore, to fulfil the requirements of the capacity-based design, the overstrength factor and the strength degradation factor are evaluated and conservative values are recommended.

* Corresponding author. Department of Engineering and Architecture, University of Trieste, Piazzale Europa 1, 34127 Trieste, Italy.

E-mail addresses: izzimatteo@gmail.com (M. Izzi), georg.flatscher@tugraz.at (G. Flatscher), massimo.fragiacomo@univaq.it (M. Fragiacomo), gerhard.schickhofer@tugraz.at (G. Schickhofer).

KEY WORDS: annular-ringed shank nail, steel-to-timber joint, Cross-Laminated Timber, hysteretic behaviour, calculation model, capacity-based design, overstrength factor, strength degradation factor.

1. INTRODUCTION

Ensuring an adequate ductility and a sufficient energy dissipation are two key aspects when designing seismic resistant multi-storey timber buildings made of Cross-Laminated Timber (CLT) panels. As a structural product, CLT is characterized by high in-plane stiffness and a linear-elastic behaviour with tendency to fail with brittle mechanism (except for compressive stresses). Therefore, mechanical connections between adjacent walls and between wall and floor panels represent the ductile zones of CLT structures, supplying most of the building flexibility and providing the necessary strength, stiffness and ductility [1].

The hysteretic behaviour of single-joints and CLT wall systems (CLT wall panel and connections) was the focus of several experimental programmes. Shear and tension tests were performed on typical metal connectors, such as hold-downs and angle brackets, and on screwed panel-to-panel connections [2-6]. Furthermore, racking tests performed on CLT walls with several layouts of connections and openings [7-12] and full-scale shaking table tests [13-15] demonstrated significant energy dissipation.

Predicting the load-carrying capacity of joints with dowel-type fasteners in CLT is more complex than for traditional sawn timber or other engineered wood products (e.g. glued laminated timber). Blaß and Uibel [16] developed a calculation model for the prediction of the fastening capacity in CLT. Specific rules for joints in CLT, derived from the works of Blaß and his collaborators, are prescribed in the Austrian National Annex to Eurocode 5 [17]. However, design formulas were not included in structural design codes of any other European country.

The experimental programme presented in the paper aims at investigating the behaviour of steel-to-timber joints with annular-ringed shank nails in CLT. These nails are used in CLT buildings to anchor typical metal connectors (such as hold-downs and angle brackets) to the wall and floor panels. Monotonic and cyclic single fastener joint shear tests were carried out in parallel and perpendicular to the face lamination of the CLT panels while nail withdrawal tests were performed from the side face of CLT panels. Moreover, the tensile strength and the yield moment of the fastener were measured via tension and bending tests, respectively.

Mechanical properties such as strength, stiffness, ductility and equivalent viscous damping ratio were assessed as prescribed in EN 12512:2001/A1 [18] and ISO 16670 [19]. Characteristic values of the experimental strength capacities were derived according to EN 14358 [20] and were compared to the analytical predictions prescribed in the current standards [21, 22, 17] and recommended in literature [16]. Finally, the overstrength factor and the strength degradation factor were evaluated and conservative values were recommended for nailed steel-to-timber joints in CLT.

2. CALCULATION MODELS

The current version of Eurocode 5 [21] prescribes design rules for traditional structural products (solid timber, glued laminated timber, etc.) and fasteners (smooth nails, dowels, bolts, etc.). However, the same standard does not include any design provision for CLT and typically used metal connectors (such as angle brackets and hold-downs) requiring the use of harmonized technical specifications like the European Technical Assessments (ETAs). Some specific rules for joints in CLT were included in the Austrian National Annex to Eurocode 5 [17]. Moreover, Blaß and Uibel [16] proposed a calculation model for joints with dowel-type fasteners in CLT, where the load-carrying capacity and the failure modes are influenced by the thickness and by the embedding strength of each board layer. It should be noticed that this model was validated on CLT panels made of board layers thinner than what are used nowadays and has not been included in structural design codes of any European country to date.

The calculation models considered in this study are described in the following sub-sections. The design rules included in Eurocode 5 [21] divide the steel-to-timber joints into two groups: joints with thin metal plates (i.e. plates with thickness less than $0.5d$, with d diameter of the fastener) and joints with thick metal plates (i.e. plates with thickness greater than d). The thickness of the metal plate influences the failure mechanism of the joint. Joints with thick plates have a ductile failure mechanism where the bending capacity of the fastener is attained with two plastic hinges together with embedding of timber. Joints with thin plates have a less ductile failure mechanism where the bending capacity is attained with one plastic hinge together with embedding of timber. It must be noticed that, due to their conical-shaped cap, annular-ringed shank nails do not have such strict distinction. For instance, ETA-13/0523 [23] (Rotho Blaas nails) takes into account a similar distinction between thin and thick plates; however, compared to Eurocode 5 [21], the condition of thick plate is satisfied with a much thinner plate (1.5 mm thickness if d = 4.0 mm and 3.0 mm thickness if d = 6.0 mm). On the contrary, the design provisions included in ETA-04/0013 [22] (Simpson Strong-Tie nails, like those used in this experimental programme) refer only to thick plates and can be applied to any joint regardless the thickness of the metal plate. Therefore, for the sake of clarity, the following discussions are all referred to steel-to-timber joints with thick plates, whereas joints with thin plates were not included in the study.

2.1. Capacity-based design approach

The application of a capacity-based design procedure to CLT structures requires the definition of specific regions that must withstand large cyclic deformations and provide a stable energy dissipation. When it comes to ductile failure of timber structures, this is achieved with proper connection design and by ensuring that no other part (less ductile or brittle) exhibits anticipated failure. However, results of past experimental programmes on metal connectors (i.e. angle brackets and hold-downs) and CLT wall systems have highlighted some inappropriate mechanisms at the connection level that may be associated to an incorrect design of the nailed steel-to-timber joints. In particular: *(a)* in wall-to-floor connections with angle brackets, failure under tensile loads due to withdrawal of the nails connected to the floor panel; *(b)* in wall-to-foundation connections with angle brackets, failure due to pull-through of the anchoring bolts; and *(c)* in wall-to-floor connections with hold-downs, tensile failure of the net cross-section of the metal sheet.

Such failure mechanisms can be avoided by applying a capacity-based design approach, both at the connection level and at the wall level. Using force-based design methods, the load flow is followed from the top to the foundation of the building and design values of the action effects are determined (E_d). At the connection level, those values are used as inputs for the ductile design of the dissipative elements. In particular and again focusing on commonly used angle brackets and hold-downs, capacity-based provisions may be employed to avoid the afore-mentioned failure mechanisms and to ensure the plasticization of laterally loaded steel-to-timber joints. Once inappropriate failures at connection level are prevented, similar provisions are applied at the wall level. Here, the strength of the CLT panel (around the connections and of the entire panel considering, e.g., openings) is designed for the overstrength of the dissipative connections considering their strength degradation for cyclic loading.

As discussed in Follesa *et al.* [24], a structural element designed in accordance with the concept of dissipative behaviour is verified at the Ultimate Limit State if:

$$E_\mathrm{d} \le \beta_\mathrm{Sd} F_\mathrm{Rd,ductile} \tag{1}$$

with E_d design value of the action effects, $F_\mathrm{Rd,ductile}$ design strength of the ductile element and β_Sd reduction factor for strength degradation for cyclic loading. The design strength of the ductile element is defined as $F_\mathrm{Rd,ductile} = k_\mathrm{mod} F_\mathrm{Rk,ductile} / \gamma_\mathrm{M}$, where $F_\mathrm{Rk,ductile}$ is its characteristic value while k_mod and γ_M represent the modification factor for duration of load and moisture content and the partial factor for material properties, respectively. Values of $F_\mathrm{Rk,ductile}$ should be determined either by theoretical considerations or from experimental results in monotonic conditions. It should be noticed that Eurocode 8 [25] sets the partial factor for material properties γ_M equal to 1.0 for ductile elements designed in accordance with the concept of dissipative behaviour.

Once the dissipative elements are verified at Ultimate Limit State, ductile failure mechanisms can be ensured by designing the strength of the brittle part ($F_\mathrm{Rd,brittle}$) so that it is greater than or equal to the strength of the ductile part ($F_{\mathrm{Rd,ductile}}$) multiplied by an overstrength factor γ_{Rd} and divided by a reduction factor for strength degradation due to cyclic loading β_{Sd} [24]:

$$\frac{\gamma_{\mathrm{Rd}}}{\beta_{\mathrm{Sd}}} F_{\mathrm{Rd,ductile}} \leq F_{\mathrm{Rd,brittle}} \tag{2}$$

with $F_{\mathrm{Rd,brittle}} = k_{\mathrm{mod}} F_{\mathrm{Rk,brittle}} / \gamma_{\mathrm{M}}$, where $F_{\mathrm{Rk,brittle}}$ is the characteristic strength of the brittle member while all the other symbols have the same meaning of those used before.

The strength degradation factor β_{Sd} takes into account the impairment of strength of the dissipative element due to cyclic loading. In the present contribution it is determined based on a statistical analysis of experimental results in cyclic conditions, i.e., as the 5$^{\mathrm{th}}$ percentile of the factor determined for every single test as follows:

$$\beta_{\mathrm{Sd}} = \frac{F_{\max(3\mathrm{rd})}}{F_{\max(1\mathrm{st})}} \tag{3}$$

where $F_{\max(1\mathrm{st})}$ and $F_{\max(3\mathrm{rd})}$ signify the strength capacities measured on the first and third envelope curves, respectively. Values of $F_{\max(1\mathrm{st})}$ and $F_{\max(3\mathrm{rd})}$ are assessed at the ‘cycle group’ (which includes three consecutive cycles at the same displacement amplitude) where the peak of the first envelope curve is achieved.

The overstrength factor γ_{Rd} accounts for all the factors that may increase the strength of the ductile element (e.g. higher-than-specified material strength, strain hardening at large deformations, commercial sections larger than what resulting from the design). It is defined as the ratio of the 95$^{\mathrm{th}}$ percentile of the experimental strength capacity $F_{\max,95}$ (in monotonic tests) to the characteristic strength of the same element $F_{\mathrm{Rk,ductile}}$ [26]:

$$\gamma_{\mathrm{Rd}} = \frac{F_{\max,95}}{F_{\mathrm{Rk,ductile}}} = \frac{F_{\max,95}}{F_{\max,05}} \cdot \frac{F_{\max,05}}{F_{\mathrm{Rk,ductile}}} = \gamma_{\mathrm{sc}} \cdot \gamma_{\mathrm{an}} \tag{4}$$

The equation above shows that γ_{Rd} can be expressed as function of two factors. The first (γ_{sc}) accounts for the scatter of strength properties in monotonic tests and is defined as the $F_{\mathrm{max,95}}$ over $F_{\mathrm{max,05}}$ ratio (95$^{\mathrm{th}}$ and 5$^{\mathrm{th}}$ percentiles of the strength property, respectively). The second factor (γ_{an}) measures the quality of the analytical model to predict the strength property and is defined as the $F_{\mathrm{max,05}}$ over $F_{\mathrm{Rk,ductile}}$ ratio, where $F_{\mathrm{max,05}}$ and $F_{\mathrm{Rk,ductile}}$ have the same meaning of those used before. Values of γ_{an} close to one means that the analytical model provides a reliable prediction of the strength property; on the contrary, ratios far from one means an analytical prediction less representative of the characteristic experimental strength.

Equation 4 clearly highlights that two different cases should be considered. Firstly, when $F_{\mathrm{Rk,ductile}}$ is determined using general rules such as those included in Eurocode 5 [21], the overstrength factor should be determined as given in Equation 4. In this situation the calculation model fully neglects some specific features of the ductile element (e.g. the profiled shank in threaded nails); therefore, it is important to consider both the approximation of the analytical model (γ_{an}) and scatter of strength properties (γ_{sc}). On the other hand, when distinct design rules are available or if the design process is based on characteristic strength capacities determined from test results, γ_{an} can be assumed equal to one and Equation 4 leads to $\gamma_{\mathrm{Rd}} = \gamma_{\mathrm{sc}}$.

2.1. Load-carrying capacity of a nailed steel-to-timber joint

Eurocode 5 [21] defines the characteristic load-carrying capacity ($F_{\mathrm{v,Rk}}$) of a nailed steel-to-timber joint as the sum of two contributions:

$$F_{\mathrm{v,Rk}} = F_{\mathrm{lat,Rk}} + 0.25 F_{\mathrm{ax,Rk}} \tag{5}$$

The first term in Equation 5 signifies the lateral dowel capacity of the joint $F_{\mathrm{lat,Rk}}$ according to the Johansen's yield theory; the second term represents the contribution due to the rope effect and is equal to 25% the withdrawal capacity of the nail $F_{\mathrm{ax,Rk}}$. Characteristic values of $F_{\mathrm{lat,Rk}}$ and $F_{\mathrm{ax,Rk}}$ are obtained with theoretical considerations and by calibration on past experimental results. The contribution due to the rope effect depends upon the connector type and is taken into account at a maximum percentage of the lateral dowel capacity $F_{\mathrm{lat,Rk}}$. For round nails with smooth shank, Eurocode 5 [21] limits the rope effect to 15% of $F_{\mathrm{lat,Rk}}$ while for other nails it is increased up to 50% of the lateral dowel capacity. The relationship presented in Equation 5 is also proposed by Blaß and Uibel [16] while ETA-04/0013 [22] increases the rope effect to 60% of the withdrawal capacity.

2.2. Lateral dowel capacity of a nailed steel-to-timber joint

Eurocode 5 [21] and ETA-04/0013 [22] adopt the European Yield Model (EYM), originally proposed by Johansen [27], to define the lateral dowel capacity of a nailed steel-to-timber joint. An ideal rigid-plastic behaviour is assumed for both the fastener's yield moment and the embedment behaviour of timber. The equations derived from this model predict the load-carrying capacity of a single fastener joint loaded in shear depending upon its geometry, the embedding strength of timber, and the yield moment of the fastener.

$$F_{\mathrm{lat,Rk}} = \min \begin{cases} f_{\mathrm{h,k}} t_1 d & \text{(a)} \\ f_{\mathrm{h,k}} t_1 d \left[\sqrt{2 + \dfrac{4M_{\mathrm{y,Rk}}}{f_{\mathrm{h,k}} t_1^2 d}} - 1 \right] & \text{(b)} \\ 2.3\sqrt{M_{\mathrm{y,Rk}} f_{\mathrm{h,k}} d} & \text{(c)} \end{cases} \tag{6}$$

The characteristic lateral dowel capacity ($F_{\mathrm{lat,Rk}}$) of a nailed steel-to-timber joint made with a thick metal plate is defined by the lowest value among those in Equation 6. The derivation of the equations has been described by Hilson [28]. The equation giving the lowest load-carrying capacity identifies the actual failure mechanism. In the previous equations, $f_{\mathrm{h,k}}$ signifies the characteristic embedding strength of timber, t_1 indicates the penetration depth while d and $M_{\mathrm{y,Rk}}$ denote the diameter and the characteristic yield moment of the fastener, respectively. Equation 6a describes a failure mechanism where the fastener behaves as a rigid element and there is only embedding of the timber member; moreover, the rope effect is not activated and has to be neglected. Equation 6b and 6c denote two failure mechanisms where the bending capacity of the fastener is attained (with one and two plastic hinges, respectively) together with embedding of the timber around the fastener. The calculation model developed by Blaß and Uibel [16] leads to formulations similar to those showed in Equation 6 where it is assumed that the CLT panels are manufactured with timber boards of the same density.

2.3. Embedding strength of timber

The embedding strength of timber depends upon several factors such as the size and cross-section shape of the fastener, the timber density and the relative orientation between applied load and timber grain [29]. Nevertheless, due to the limited size of the nail cross-section, the models discussed below do not take into the account this last variable.

Eurocode 5 [21] and ETA-04/0013 [22] define the characteristic embedding strength of timber $f_{\mathrm{h,k}}$ depending upon the characteristic density of the timber ρ_{k} and the diameter of the fastener d ; the model (Equation 7) was derived by Whale *et al.* [30] for a smooth nail embedded in a solid timber element without predrilled hole.

$$f_{\mathrm{h,k}} = 0.082\rho_{\mathrm{k}} d^{-0.3} \tag{7}$$

The other two models considered in the study were derived by Uibel and Blaß [31] from the results of embedment tests in CLT panels. The first one provides a general formulation for the prediction of the embedding strength (Equation 8); the latter one (Equation 9) is used in the Austrian National Annex to Eurocode 5 [17] for profiled nails placed in CLT and is derived from Equation 8 by considering a characteristic density ρ_{k} = 400 kg/m^3 :

$$f_{\mathrm{h,k}} = 0.112\rho_{\mathrm{k}}^{1.05} d^{-0.5} \tag{8}$$

$$f_{\mathrm{h,k}} = 60 d^{-0.5} \tag{9}$$

2.4. Yield moment of the fastener

The yield moment of the fastener is an important parameter in the design of steel-to-timber joints according to Eurocode 5 [21]. Johansen [27] assumed it as the elastic moment capacity of the circular cross-section; the possible increase of capacity associated to plastic deformations was disregarded. However, an ideal rigid-plastic behaviour was adopted in the subsequent developments of his theory.

The first model considered in the study has been proposed by Blaß and Colling [32] and defines the yield moment of the fastener as the plastic moment capacity of the circular cross-section:

$$M_{\mathrm{y,Rk}} = f_{\mathrm{y,k}} d^3 / 6 \qquad (10)$$

In the previous equation the symbol $f_{\mathrm{y,k}}$ indicates an “equivalent” yield strength, estimated as 90% the characteristic ultimate tensile strength $f_{\mathrm{u,k}}$ while d is the diameter of the fastener. The ultimate tensile strength $f_{\mathrm{u,k}}$ depends upon the quality of the wire from which the fastener was manufactured and has to be evaluated with experimental tests.

Based on the results of an experimental programme on joints with dowel-type fasteners, Blaß *et al.* [33] reported that most of the failures occurred for low values of the fasteners’ bending angle (significantly below 45°). Therefore, the plastic capacity of the dowel’s cross-section was not attained and the yield moment was lower than according to EN 409 [34]. Hence, Blaß *et al.* [33] proposed a calculation model which is currently prescribed in Eurocode 5 [21], ETA-04/0013 [22] and Blaß and Uibel [16]. The model is based on a theoretical derivation of the fastener’s bending angle at a joint slip of 15 mm and defines the yield moment as given in Equation 11, depending upon the diameter d and a minimum tensile strength $f_{\mathrm{u,k}}$ = 600 N/mm^2:

$$M_{\mathrm{y,Rk}} = 0.30 f_{\mathrm{u,k}} d^{2.6} \qquad (11)$$

Due to strain hardening and the varying effects of profiling, specific calculation models for threaded nails have not been derived; for a realistic joint design, the actual yield moment of those fasteners has to be determined with experimental tests as prescribed in EN 409 [34].

2.5. Axial withdrawal capacity of a nailed joint

Eurocode 5 [21] and ETA-04/0013 [22] define the axial withdrawal capacity ($F_{\mathrm{ax,Rk}}$) of a nailed joint depending upon the withdrawal parameter $f_{\mathrm{ax,k}}$, the diameter of the fastener d and the profiled length of the shank l_{thr}:

$$F_{\mathrm{ax,Rk}} = f_{\mathrm{ax,k}} l_{\mathrm{thr}} d \tag{12}$$

The current version of the Eurocode 5 [21] does not provide any rule for predicting the withdrawal parameter of threaded nails and the use of harmonized technical specifications is required. Specific design rules for Simpson Strong-Tie connector nails have been included in ETA-04/0013 [22] and estimate $f_{\mathrm{ax,k}}$ as given in Equation 13, depending upon the geometry of the fastener (threaded length and diameter) and the characteristic density of timber.

$$f_{\mathrm{ax,k}} = \min \begin{cases} 6.125\left(1+\dfrac{1.5d}{l_{\mathrm{thr}}}\right)\left(\dfrac{\rho_{\mathrm{k}}}{350}\right) \\ \left(10.92-0.0158d-0.0968l_{\mathrm{thr}}\right)\left(\dfrac{\rho_{\mathrm{k}}}{320}\right)^2 \end{cases} \tag{13}$$

The other two models considered in the study were derived by Blaß and Uibel [16] in the case of a profiled nail embedded in the side face of a CLT panel. The first model provides a general formulation for the prediction of the withdrawal capacity (Equation 14). The latter (Equation 15) is currently included in the Austrian National Annex to Eurocode 5 [17] and is obtained from Equation 14 by assuming a characteristic density ρ_{k} = 400 kg/m^3.

$$F_{\mathrm{ax,Rk}} = 0.117 d^{0.6} l_{\mathrm{thr}} \rho_{\mathrm{k}}^{0.8} \tag{14}$$

$$F_{\mathrm{ax,Rk}} = 14 d^{0.6} l_{\mathrm{thr}} \tag{15}$$

2.6. Slip modulus of a nailed joint

Eurocode 5 [21] provides a calculation model for the prediction of the instantaneous slip modulus of a timber-to-timber joint (K_{ser}). The derivation of the model is described in Ehlbeck and Larsen [35]. Therein, the instantaneous slip modulus is defined as the secant modulus of the load-displacement curve at approximately 40% of the characteristic load-carrying capacity of the joint. For nailed steel-to-timber joints, based on mechanical relationships, Eurocode 5 [21] suggests that the slip modulus of a similar timber-to-timber joint may be doubled up. The resulting model predicts the instantaneous slip modulus K_{ser} depending upon the average density of timber ρ_{m} and the diameter of the nail d :

$$K_{\text{ser}} = 2\rho_m^{1.5} d^{0.8} / 30 \tag{16}$$

3. EXPERIMENTAL PROGRAMME

3.1. Materials

Tests were performed using annular-ringed shank nails (Figure 1a) produced by Simpson Strong-Tie [22]. Each nail has a total length of 60 mm and a penetration depth t_1 = 54 mm. The threaded shank, of length l_{thr} = 44 mm, increases the withdrawal strength under axial loads while the conical-shaped cap enhances the clamping to the metal plate and enforces a ductile failure mechanism with two plastic hinges. The nails are cold-formed from a steel wire with nominal diameter d = 4.0 mm; due to the profiling, the inner diameter of the threaded shank is 3.6 mm whereas the outer diameter is equal to 4.2 mm.

Solid timber panels made of five crosswise laminated board layers (CLT) and a total thickness of 134 mm (**26**-27-**28**-27-**26**) were used in the tests (Figure 1b). The numbers in brackets denote the thickness of each board layer; the bold notation was used to mark the layers with boards parallel to the face lamination of the panel. As prescribed in EN 1380 [36], the panels were conditioned at 20°C temperature and 65% relative humidity before performing the tests.

3.2. Tension tests and bending tests

The ultimate tensile strength and the yield moment of the fasteners were investigated with five tension tests and ten bending tests, respectively. The tension tests were carried out in displacement control until failure (Figure 2a); due to the small cross-section of the fastener, a thin metal pipe was placed around the nail shank to increase the clamping to the testing machine and to avoid issues with the experimental setup. The bending tests were performed in displacement control until a rotation of 45° (Figure 2b); the experimental setup was similar to the configuration depicted in Appendix A of EN 409 [34]. A free bending length of three times the diameter was ensured in all the tests.

3.3. Nail withdrawal tests

The withdrawal capacity of the nailed joint was investigated with twenty-two nail withdrawal tests, carried out in accordance with EN 1382 [37]. The experimental setup consists of a nail embedded in the side face of a CLT panel and clamped to the testing machine (Figure 2c). The load bearing capacity was measured with a load cell, placed between the moving crosshead of the testing machine and the clamp which the nail was restrained to; the local displacements of the nail were measured with two linear variable displacement transducers (LVDTs) in the proximity of the nail cap (Figure 3a). Tests were carried out in displacement control at a rate of 2 mm/min and were stopped after a 40% loss of the maximum load bearing capacity.

3.4. Single fastener joint shear tests

The lateral load bearing capacity and the hysteretic behaviour of the nailed steel-to-timber joint were investigated with shear tests. Six monotonic tests plus fifteen cyclic tests (labelled series SH00 and SH00-C, respectively) were carried out parallel to the face lamination of the CLT panel; furthermore, five monotonic tests plus fifteen cyclic tests (labelled series SH90 and SH90-C, respectively) were performed in the perpendicular direction. Tests were carried out in accordance with EN 1380 [36]; a symmetric setup was adopted, with two nails embedded at the same location in the opposite side faces of the CLT panel (Figure 2d). The load was applied to the nails cap with two 4 mm thick metal plates obtained by cutting the shoulders of two hold-downs; to minimize the initial friction between the metal plates and the timber surfaces, thin metal blades were interposed among those elements while driving the nails into the CLT panel and removed just before testing. The load bearing capacity of the nailed joint was measured with a load cell, incorporated between the moving crosshead of the testing machine and the steel element to which the metal plates were restrained; the local displacements of the nails were measured with two LVDTs, restrained in correspondence of the nail caps (Figure 3b).

The loading protocol of the monotonic tests was defined in accordance with EN 26891 [38]; an estimated maximum load of 9.0 kN (4.5 kN for each nail) was assumed in both series. Load control with an input loading rate of 1.8 kN/min was used up to 70% of the estimated maximum load; displacement control at a rate of 4 mm/min was used afterwards.

The displacement histories of the cyclic tests were defined according to ISO 16670 [19], acquiring the average ultimate displacements of each monotonic test series. The method proposed by ISO 16670 [19] was preferred to the one prescribed in EN 12512:2001/A1 [18] to avoid issues related to the lack of a standardized definition of the yield displacement [39, 40]. For each series, the first eleven tests were performed with the displacement levels prescribed by ISO 16670 [19] (one single cycle for 1.25-2.50-5.00-7.50-10% of the ultimate displacement; three cycles from 20% to 100% of the ultimate displacement, with 20% steps). To generate suitable data for calibration of the hysteresis models, the last four tests of each series were carried out with a modified set of displacement levels (same schedule for the single cycles; from 20% to 100% of the ultimate displacement, with 10% steps where three cycles at the same target displacement are applied). An input displacement rate varying from 1 to 2 mm/min was used in all the tests.

3.5. Assumptions on data analysis

The mechanical properties of the joint tests were assessed according to EN 12512:2001/A1 [18] and ISO 16670 [19]. Figure 4 shows the model given in EN 12512:2001/A1 [18], used to evaluate the mechanical properties from the monotonic tests and from the first envelope curves of the cyclic tests.

In the monotonic tests (Figure 4), the maximum load bearing capacity (peak strength) and the displacement at which this is attained are denoted with F_{max} and V_{max}. The symbol K_{ser} signifies the instantaneous slip modulus of the joint, given by the slope of the line drawn through the points of the loading curve at 10% and 40% of F_{max}; F_{y} and V_{y} denote the yield load and its displacement while the ultimate load and its displacement are denoted with F_{u} and V_{u}, respectively. The yield point is determined by the intersection of the line used to define K_{ser} and the tangent line to the loading curve with slope equal to $K_{\text{ser}}/6$; the ultimate displacement is taken as either the displacement at failure or the displacement at 80% of F_{max}, whichever occurs first. Finally, the ductility ratio of the joint (denoted as $Duct$) is evaluated as the V_{u} to V_{y} ratio.

In the cyclic tests, the envelope curves of the hysteresis loops are derived by connecting the points at maximum load in the first, second and third cycles, respectively; however, in the first five single cycles the same values of the maximum load are taken for all the envelope curves. The maximum load bearing capacity, the slip modulus and the other mechanical properties mentioned for the monotonic tests are derived from the first envelope curve. Moreover, the peak strength is also extracted from the third envelope curve ($F_{\text{max(3rd)}}$). The strength degradation factor due to cyclic loading (β_{Sd}) is assessed at the cycle group where the maximum strength of the first envelope curve is achieved and is determined as the ratio of the strength on the third envelope curve to its corresponding value on the first envelope curve. If the strength on the third envelope curve is not available for that cycle group, β_{Sd} is evaluated on the preceding cycle group. The equivalent viscous damping ratio is calculated as $\nu_{\text{eq}} = E_{\text{diss}}/(4\pi E_{\text{pot}})$, with E_{diss} dissipated energy per full cycle and E_{pot} available potential energy as given in EN 12512:2001/A1 [18]. This method is preferred to the one included in the standard as it can be used for different curve shapes in the negative part of the loading curve. As suggested by Flatscher *et al.* [2], the available potential energy E_{pot} is derived from a second set of envelope curves obtained by connecting the points of maximum displacement per cycle. The equivalent viscous damping ratio at the first ($\nu_{\mathrm{eq(1st)}}$) and third loop ($\nu_{\mathrm{eq(3rd)}}$) is determined as the average values of all entire cycle groups before the ultimate displacement V_{u} was attained.

Average values (μ) and the coefficients of variation ($COV[\mu]$) are derived for all the mechanical properties; furthermore, characteristic values of the experimental strength capacities (5th percentile) are calculated in accordance with EN 14358 [20] (Equation 17) assuming a log-normal distribution.

$$x_{05} = \exp\left(\overline{\mu} - k_{\mathrm{s}} \cdot \overline{\sigma}\right) \tag{17}$$

In the equation above, the average value and the corrected sample standard deviation of the natural logarithm distribution are denoted with $\overline{\mu}$ and $\overline{\sigma}$, respectively. The k_{s} factor is an operator associated to the 5th percentile (x_{05}); its value depends upon the number of data available and is given in a tabular form in EN 14358 [20]. The 95th percentiles of the strength capacities (x_{95}) were obtained by inverting the sign of the k_{s} factor.

3.6. Measurement of moisture content and density of the CLT panels

Measurements of moisture content (MC) and density (ρ) of the CLT panels were taken either in the proximity (shear tests) or at the location (withdrawal tests) of the nail in the tests. The MC is measured with the oven dry method [41] by analysing altogether 59 test specimens (5 for series SH00, 12 for SH00-C, 5 for SH90, 15 for SH90-C and 22 for the withdrawal tests). For each series, average values of density at 12% MC are determined in accordance with EN 384 [42] while characteristic values of density are determined by means of Equation 17.

4. RESULTS AND DISCUSSIONS

4.1. Tension tests and bending tests

Table 1 lists average values and coefficients of variation of the strength capacities obtained from the tension tests and from the bending tests; results are expressed in terms of ultimate tensile strength f_{u} and yield moment M_{y}. Table 2 presents the characteristic strength capacities computed from the test results and a comparison with the calculated values of the yield moment. The subscript 05 is used to denote the 5$^{\mathrm{th}}$ percentile of the strength whereas 95 identifies its 95$^{\mathrm{th}}$ percentile, respectively. The characteristic strength values were assessed from the experimental data as prescribed in EN 14358 [20] assuming k_{s} = 2.460 for the tension tests and k_{s} = 2.100 for the bending tests.

All the fasteners used in the tension tests (Figure 5a) failed in a brittle manner in correspondence of the inner diameter of the profiled shank; however, to be consistent with Eurocode 5 [21], the ultimate tensile strength f_{u} was defined as the ratio of maximum load to the nominal area of the shank (with diameter d). As visible in Table 2, the tensile strength $f_{\mathrm{u,05}}$ is slightly higher than the value suggested in the reference standards [21, 22, 17] and literature [16] (i.e. $f_{\mathrm{u,k}}$ = 600 N/mm^2).

Evident signs of failure were not visible in any of the fasteners tested in bending; a fully developed plastic hinge was recognised on some specimens while others showed a partially grown plastic hinge and a distributed plastic deformation (Figure 5b). As prescribed in EN 409 [34], the yield moment M_{y} should be determined either as the peak of the experimental moment-rotation relationship or as the moment at 45° rotation angle. However, due to some issues with the experimental setup, some tests were stopped between 40° and 45° and the yield moment was assessed assuming an ultimate rotation of 40°. The afore-mentioned issues were caused by the deformed shape of the fastener, which limited the rotational capacity of the test setup. This is clearly visible in Figure 2b, where the moving part of the setup touched its fixed section before reaching a rotation of 45°. However, since the peak strength of the moment-rotation relationship was generally attained before 40°, the results were not affected by this issue.

Calculated values of the yield moment were determined assuming $f_{u,k}$ = 600 N/mm^2. The model proposed by Blaß and Colling [32] ($M_{y,Rk\ B\&C}$) provided a more reliable prediction compared to the Eurocode 5 [21] model ($M_{y,Rk\ EC5}$). Nevertheless, calculated values are much higher compared to the experimental result (more than 25%). As pointed out in Section 2.4, specific calculation models to predict the yield moment of fasteners with profiled shank have not been derived yet; therefore, the comparison given in Table 2 is of particular interest, as it gives an insight into the reliability of current design rules for the prediction of the yield moment of an annular-ringed shank nail. It should be noticed that the scatter of results in the bending tests is approximately ten times higher than in the tension tests; this suggests that the residual stresses produced by cold forming might have an influence on the bending behaviour of the nail. Results might also be affected by the limited number of tests performed. As a consequence, future studies should consider a wider set of test results and should investigate the bending behaviour of the nail under cyclic conditions.

4.2. Nail withdrawal tests

The mechanical properties resulting from the nail withdrawal tests are summarized in Table 3 while the characteristic strength capacities computed from the tests and a comparison with the calculated values are given in Table 4. Figure 6 provides a comparison among all the experimental results (grey solid lines) and the trilinear approximating curve (red dashed line) determined by the average values given in Table 3; the trilinear approximating curve connects origin, yield, peak and ultimate strength. The experimental loading curves show a linear fashion until the yield load, a clear maximum and a distinct load decrease after the displacement corresponding to the peak strength.

Characteristic strength values from the tests and the characteristic density of the CLT panels (used as input parameter in the analytical models) were assessed as prescribed in EN 14358 [20] assuming k_s = 1.918. The model developed by Blaß and Uibel [16] ($F_{ax,Rk\ B\&U}$) gave the best agreement with the experimental results. ETA-04/0013 [22] ($F_{ax,Rk\ ETA}$) led to slightly less accurate values while the rules included in the Austrian National Annex to Eurocode 5 [17] ($F_{\mathrm{ax,Rk\,ÖN}}$) provided a more conservative prediction of the load-carrying capacity. In this context it must be noticed that, for design purposes, the Austrian National Annex to Eurocode 5 [17] suggests the use of only 80% of $F_{\mathrm{ax,Rk}}$ if the diameter d is smaller than 6 mm. Furthermore, as mentioned in Section 2.5, Eurocode 5 [21] and ETA-04/0013 [22] adopt the same model for the prediction of the axial withdrawal capacity; however, the former does not provide any information on the withdrawal parameter and the use of harmonized technical specifications is required.

Based on the results presented in Table 4, values of γ_{sc} and γ_{an} were evaluated for nailed joints loaded in withdrawal. The first parameter (γ_{sc}) was determined as the $F_{\mathrm{max,95}}$ to $F_{\mathrm{max,05}}$ ratio and is equal to 1.76. The latter parameter (γ_{an}) was defined as the $F_{\mathrm{max,05}}$ over $F_{\mathrm{ax,Rk\,ÖN}}$ ratio, where $F_{\mathrm{ax,Rk\,ÖN}}$ is the calculated strength capacity according to the Austrian National Annex to Eurocode 5 [17], and is equal to 1.13. Therefore, an overstrength factor γ_{Rd} = 2.0 is recommended for nailed joints with annular-ringed shank nails loaded in withdrawal when $F_{\mathrm{ax,Rk}}$ is defined using general rules (e.g. those included in the above-mentioned standard) while γ_{Rd} = 1.8 is recommended if the design is based on the characteristic strength capacities determined from test results. It should be noticed that the overstrength factors determined on the results of single nails loaded in withdrawal are not necessarily valid also for a group of nails. In particular, they could be even lower for, e.g., a metal connector which is anchored to the panel with several nails that bear simultaneously the load.

The load bearing mechanism of the nailed joint loaded in withdrawal depends upon the friction between threaded shank and the surrounding timber. This mechanism is activated when the steel plate (to which the nail is clamped) is lifted from the CLT panel (in which the nail is embedded). Once the nail is extracted from the CLT panel, it cannot be pushed back by the steel plate; this suggests that the load bearing mechanism in withdrawal is effective as long as the joint is subjected to monotonic loads while is very weak in cyclic conditions and, if possible, it should be avoided. As already mentioned, applying the capacity-based design approach and over-strengthening this part of the connection via, e.g., the use of more nails or by equipping it with screws instead of nails, might be a proper solution.

4.3. Single fastener joint shear tests

Average values and coefficients of variation of the mechanical properties obtained from the shear tests are listed in Table 5 (monotonic) and in Table 6 (cyclic), respectively. Results are presented both in parallel and in perpendicular direction to the face lamination of the CLT panels. Table 7 presents the characteristic strength capacities computed from the monotonic tests and a comparison with the analytical models discussed in Section 2. Figures 7a-7b show a comparison among the results of the monotonic tests (grey solid lines) and the trilinear approximating curve determined by the average quantities given in Table 5 (red dashed line connecting origin, yield, peak and ultimate strength). The same figures show also the instantaneous slip modulus of the steel-to-timber joint (dark grey dashed line), determined according to Equation 16. Figures 8a-8b show a comparison among the first envelope curves extracted from the cyclic tests (grey solid lines) and the trilinear approximating curve determined by the average values given in Table 6 (red dashed line). For comparison with the monotonic tests, the same figures show also the trilinear approximating curves determined by the quantities given in Table 5 (dark grey dashed line).

The peak strength of both monotonic series was achieved at approximately 13 mm of displacement. The instantaneous slip modulus and the peak strength in perpendicular direction are slightly higher than in the parallel direction whereas the ultimate displacement and the ductility are lower. Moreover, the peak strengths of the cyclic tests are lower than the quantities determined in monotonic conditions. It should be also noticed that some tests have failed prior to the cycle group where the maximum strength of the monotonic tests was achieved (as visible in Figures 8a-8b).

Two plastic hinges can be recognised in all the fasteners, one under the cap and another one in the shank (10 to 15 mm below). In the monotonic tests, failures always occurred for tearing of the cap in one fastener due to a combination of tension and bending (Figure 9a). In the cyclic tests, four different failure mechanisms can be recognised (Figure 9b): (*a*) tearing of the cap, (*b*) failure in bending, (*c*) failure in bending with a partially torn cap, (*d*) failure in bending with tearing of the cap. CLT panels tested in parallel direction to the face lamination failed for excess of embedment while local splitting occurred in some specimens loaded in perpendicular direction.

Characteristic strength values were computed from the experimental data in accordance with EN 14358 [20] assuming k_s = 2.388 for series SH00, k_s = 2.460 for series SH90 and k_s = 1.990 for both series SH00-C and SH90-C. Furthermore, the characteristic densities of the CLT panels used in test series SH00 and SH90 (required as input parameter for the analytical models) were determined according to the same standard assuming k_s = 2.460. All the calculation models led to conservative predictions of the load-carrying capacity. The rules included in ETA-04/0013 [22] ($F_{\text{v,Rk ETA}}$) provided the best agreement with the experimental results. ÖNORM B 1995-1-1 [17] ($F_{\text{v,Rk ÖN}}$) and the model by Blaß and Uibel [16] ($F_{\text{v,Rk B\&U}}$) led to slightly less accurate values while Eurocode 5 [21] ($F_{\text{v,Rk EC5}}$) gave the most conservative predictions. It is important to note that the load-carrying capacity of ETA-04/0013 [22] and Eurocode 5 [21] were computed using the same input values of $F_{\text{lat,Rk}}$ and $F_{\text{ax,Rk}}$. However, Eurocode 5 [21] considers a contribution due to the rope effect equal to 25% of the withdrawal capacity (Equation 5) while ETA-04/0013 [22] increases that effect up to 60% of $F_{\text{ax,Rk}}$.

Similarly to what done in Section 4.2, values of γ_{sc} and γ_{an} were evaluated for laterally loaded steel-to-timber joints considering the Austrian National Annex to Eurocode 5 [17] ($F_{\text{v,Rk ÖN}}$) as the reference standard. Based on the results presented in Table 7, γ_{sc} is equal to 1.27 and γ_{an} to 1.44 in parallel to the face lamination of the CLT panel while γ_{sc} = 1.53 and γ_{an} = 1.48 in the perpendicular direction. Therefore, the following overstrength factors are recommended: if $F_{\text{v,Rk}}$ is defined using general rules (e.g. those included in the Austrian National Annex to Eurocode 5 [17]), γ_{Rd} = 1.8 should be assumed parallel to the face lamination of CLT panel and γ_{Rd} = 2.3 in the perpendicular direction. If the design is based on the characteristic strength capacities determined from test results, γ_{Rd} = 1.3 should be assumed parallel to the face lamination of CLT panel and γ_{Rd} = 1.5 in the perpendicular direction.

The 5$^{\mathrm{th}}$ and 95$^{\mathrm{th}}$ percentiles of the strength degradation factor were assessed from the experimental data as prescribed in EN 14358 [20]; $\beta_{\mathrm{Sd},05}$ is equal to 0.60 and $\beta_{\mathrm{Sd},95}$ to 0.83 parallel to the superficial lamination of the CLT panel while $\beta_{\mathrm{Sd},05}$ = 0.54 and $\beta_{\mathrm{Sd},95}$ = 0.94 in the perpendicular direction. Based on the statistical analysis, a conservative strength degradation factor β_{Sd} = 0.6 is recommended for laterally loaded steel-to-timber joints in parallel to the face lamination of the CLT panel while β_{Sd} = 0.5 is recommended in the perpendicular direction.

Once more it should be noticed that both the overstrength factors and the strength degradation factors were determined using results of laterally loaded steel-to-timber joints equipped with one single nail and could be even lower as each connector is usually anchored to a CLT panel with several fasteners that bear simultaneously the load.

Finally, the experimental slip moduli of the monotonic tests (given in Table 5) are compared to the calculated values according to Equation 16. The predicted instantaneous slip modulus in parallel direction to the superficial lamination of the CLT panel is equal to 2108 N/mm while in perpendicular direction is equal to 1962 N/mm; the discrepancy between the calculated values depends upon the mean densities of the respective samples. However, the results computed from the experimental data are significantly lower than the analytical predictions. This suggests that the assumption of a rigid metal plate, which is the basis for doubling the stiffness of steel-to-timber joints according to Eurocode 5 [21], might not be valid for the conducted tests, especially at low load levels.

CONCLUSIONS

This paper investigates the mechanical behaviour of steel-to-timber joints with annular-ringed shank nails in CLT. Monotonic and cyclic shear tests were performed on single fastener joints loaded in parallel and perpendicular direction to the face lamination of the CLT panels; furthermore, withdrawal tests were carried out on single nails embedded in the side face of CLT panels. Finally, the ultimate tensile strength and the yield moment of the fastener were determined by performing tension tests and bending tests, respectively. Characteristic values of the strength capacities were assessed from the experimental data and compared to the values calculated according to the current design models.

The best agreement with the experimental results was obtained with the design provisions included in the European Technical Assessment (ETA) of the fasteners tested [22]. The model developed by Blaß and Uibel [16] led to slightly less accurate values while the rules included in Eurocode 5 [21] and in the Austrian National Annex to Eurocode 5 [17] provided more conservative predictions of the load-carrying capacity. Finally, it was shown that the model included in Eurocode 5 [21] for the prediction of the instantaneous slip modulus of a nailed steel-to-timber joint significantly overestimates the experimental results.

Based on the statistical analysis, the overstrength and strength degradation factors of the joints with annular-ringed shank nails were evaluated. For each configuration, two overstrength factors were determined: one is recommended when the characteristic load-carrying capacity is defined based on general rules (e.g. those included in the Austrian National Annex to Eurocode 5 [17]); the other is recommended when the design is based on the characteristic strength capacities determined from test results. Based on the previous assumptions, γ_{Rd} = 2.0 and γ_{Rd} = 1.8 are recommended for nailed joints with annular-ringed shank nails loaded in withdrawal. The values γ_{Rd} = 1.8 and γ_{Rd} = 1.3 are recommended for laterally loaded steel-to-timber joints parallel to the face lamination of the CLT panel, while the values γ_{Rd} = 2.3 and γ_{Rd} = 1.5 should be assumed in the perpendicular direction.

The strength degradation factors were also determined for the laterally loaded steel-to-timber joints and conservative values of β_{Sd} = 0.6 and β_{Sd} = 0.5 are recommended in parallel and perpendicular direction to the face lamination of the CLT panel, respectively. The overstrength and the strength degradation factors significantly depend on the scatter of mechanical properties observed in the tests and were determined on the results of single fastener joints. Due to the group effect, this scatter might be lower for, e.g., a metal connector anchored to the CLT panel with a group of nails. Therefore, in these situations, both factors may be even lower.

ACKNOWLEDGEMENTS

The study periods of Matteo Izzi, as a visiting scholar at the Institute of Timber Engineering and Wood Technology, Graz University of Technology (Graz, Austria), were financially supported by the COST Actions FP1004 and FP1402. The Management Committees of the COST Actions and the representatives of COST Office are gratefully acknowledged for the research grants, which contributed to a successful outcome of this study. This research was completed while Matteo Izzi was collaborating as Research Assistant at the Trees and Timber Institute of San Michele all’Adige (Italy), the financial support of which is gratefully acknowledged.

REFERENCES

1. Fragiacomo M, Dujic B, Sustersic I (2011) Elastic and ductile design of multi-storey crosslam massive wooden buildings under seismic actions. *Engineering structures,* **33**(11): 3043-3053, doi: 10.1016/j.engstruct.2011.05.020.

2. Flatscher G, Bratulic K, Schickhofer G (2015) Experimental tests on cross-laminated timber joints and walls. *Proceedings of the ICE - Structures and Buildings,* **168**(11): 868-877, doi: 10.1680/stbu.13.00085.

3. Gavric I, Fragiacomo M, Ceccotti A (2015) Cyclic behaviour of typical metal connectors for cross laminated (CLT) structures. *Materials and Structures,* **48**(6): 1841-1857, doi: 10.1617/s11527-014-0278-7.

4. Gavric I, Fragiacomo M, Ceccotti A (2015) Cyclic behavior of typical screwed connections for cross-laminated (CLT) structures. *European Journal of Wood and Wood Products*, **73**(2): 179-191, doi: 10.1007/s00107-014-0877-6.

5. Joyce T, Smith I, Ballerini M (2011) Mechanical behaviour of in-plane shear connections between CLT wall panels. *44th CIB-W18 Meeting*, Alghero, Italy, Paper 44-7-2.

6. Tomasi R, Smith I (2015) Experimental Characterization of Monotonic and Cyclic Loading Responses of CLT Panel-To-Foundation Angle Bracket Connections. *Journal of Materials in Civil Engineering*, **27**(6): 04014189(1-10), doi: 10.1061/(ASCE)MT.1943-5533.0001144.

7. Dujic B, Pucelj J, Zarnic R (2004) Testing of Racking Behavior of Massive Wooden Wall Panels. *37th CIB-W18 Meeting*, Edinburgh, Scotland, Paper 37-15-2.

8. Dujic B, Aicher S, Zarnic R (2005) Racking of Wooden Walls Exposed to Different Boundary Conditions. *38th CIB-W18 Meeting*, Karlsruhe, Germany, Paper 38-15-6.

9. Dujic B, Klobcar S, Zarnic R (2007) Influence of Openings on Shear Capacity of Wooden Walls. *40th CIB-W18 Meeting*, Bled, Slovenia, Paper 40-15-6.

10. Gavric I, Fragiacomo M, Ceccotti A (2015) Cyclic Behavior of CLT Wall Systems: Experimental Tests and Analytical Prediction Models. *Journal of Structural Engineering*, **141**(11): 04015034(1-14), doi: 10.1061/(ASCE)ST.1943-541X.0001246.

11. Hummel J, Flatscher G, Seim W, Schickhofer G (2013) CLT Wall Elements Under Cyclic Loading - Details for Anchorage and Connection. *COST Action FP1004, Focus solid timber solutions - European Conference on Cross Laminated Timber (CLT)*, pp: 152-165, Graz, Austria.

12. Popovski M, Karacabeyli E (2011) Seismic Performance of Cross-Laminated Wood Panels. *44th CIB-W18 Meeting*, Alghero, Italy, Paper 44-15-7.

13. Ceccotti A, Sandhaas C, Okabe M, Yasumura M, Minowa C, Kawai N (2013) SOFIE project - 3D shaking table test on a seven-storey full-scale cross-laminated building. *Earthquake Engineering & Structural Dynamics*, **42**(13): 2003-2021, doi: 10.1002/eqe.2309.

14. Flatscher G, Schickhofer G (2015) Shaking-table test of a cross-laminated timber structure. *Proceedings of the ICE - Structures and Buildings*, **168**(11): 878-888, doi: 10.1680/stbu.13.00086.

15. Hristovski V, Dujic B, Stojmanovska M, Mircevska V (2013) Full-Scale Shaking-Table Tests of XLam Panel Systems and Numerical Verification: Specimen 1. *Journal of Structural Engineering*, **139**(11): 2010-2018, doi: 10.1061/(ASCE)ST.1943-541X.0000754.

16. Blaß HJ, Uibel T (2007) *Tragfähigkeit von stiftförmigen Verbindungsmitteln in Brettsperrholz*. **8**, Karlsruher Berichte zum Ingenieurholzbau, Karlsruhe, Germany, doi: 10.5445/KSP/1000006318.

17. ÖNORM B 1995-1-1 (2014) Eurocode 5. Bemessung und Konstruktion von Holzbauten. Teil 1-1: Allgemeines. Allgemeine Regeln und Regeln für den Hochbau. Nationale Festlegungen zur Umsetzung der ÖNORM EN 1995-1-1 nationale Erläuterungen und nationale Ergänzungen. ÖN, Wien, Austria.

18. EN 12512:2001/A1 (2005) Timber structures. Test methods. Cyclic testing of joints made with mechanical fasteners. CEN, Brussels, Belgium.

19. ISO 16670 (2003) Timber Structures. Joints made with mechanical fasteners. Quasi-static reversed-cyclic test method. ISO, Geneva, Switzerland.

20. EN 14358 (2006) Timber structures. Calculation of characteristic 5-percentile values and acceptance criteria for a sample. CEN, Brussels, Belgium.

21. EN 1995-1-1:2004/A2 (2014) Eurocode 5: Design of timber structures. Part 1-1: General. Common rules and rules for buildings. CEN, Brussels, Belgium.

22. ETA-04/0013 (2015) European Technical Assessment. Nails and screws for use in nailing plates in timber structures. ETA-Denmark, Nordhavn, Denmark.

23. ETA-13/0523 (2013) European Technical Assessment. Annular ring shank nails and connector screws. ETA-Denmark, Nordhavn, Denmark.

24. Follesa M, Fragiacomo M, Vassallo D, Piazza M, Tomasi R, Rossi S, Casagrande D (2015) A proposal for a new Background Document of Chapter 8 of Eurocode 8. *INTER 2015 Meeting*, Šibenik, Croatia, Paper 48-7-3.

25. EN 1998-1:2004/A1 (2013) Eurocode 8: Design of structures for earthquake resistance. Part 1: General rules, seismic actions and rules for buildings. CEN, Brussels, Belgium.

26. Jorissen A, Fragiacomo M (2011) General notes on ductility in timber structures. *Engineering structures*, **33**(11): 2987-2997, doi: 10.1016/j.engstruct.2011.07.024.

27. Johansen KW (1949) Theory of timber connections. *International Association of Bridge and Structural Engineering,* **9**: 249-262, doi: 10.5169/seals-9703.

28. Hilson BO (1995) Joints with dowel-type fasteners - Theory. *Timber Engineering STEP 1: Basis of design, material properties, structural components and joints*, pp: C3/1-11, Centrum Hout, Almere, The Netherlands.

29. Zhou T, Guan Z (2006) Review of existing and newly developed approaches to obtain timber embedding strength. *Progress in Structural Engineering and Materials,* **8**(2): 49-67, doi: 10.1002/pse.213.

30. Whale LRJ, Smith I, Hilson BO (1989) Characteristic properties of nailed and bolted joints under short-term lateral load, Part 4 - The influence of testing mode and fastener diameter upon embedment test data. *Journal of the Institute of Wood Science,* **11**(5): 156-161.

31. Uibel T, Blaß HJ (2006) Load Carrying Capacity of Joints With Dowel Type Fasteners in Solid Wood Panels. *39th CIB-W18 Meeting*, Florence, Italy, Paper 39-7-5.

32. Blaß HJ, Colling F (2015) Load-carrying capacity of dowelled connections. *INTER 2015 Meeting*, Šibenik, Croatia, Paper 48-7-3.

33. Blaß HJ, Bienhaus A, Krämer V (2001) Effective Bending Capacity of Dowel-Type Fasteners. *International RILEM Symposium on Joints in Timber Structures*, Cachan, France.

34. EN 409 (2009) Timber structures. Test methods. Determination of the yield moment of dowel type fasteners. CEN, Brussels, Belgium.

35. Ehlbeck J, Larsen HJ (1993) Eurocode 5 - Design of Timber Structures: Joints. *International Workshop on Wood Connectors*, Madison, Wisconsin, USA.

36. EN 1380 (2009) Timber structures. Test methods. Load bearing nails, screws, dowels and bolts. CEN, Brussels, Belgium.

37. EN 1382 (1999) Timber structures. Test methods. Withdrawal capacity of timber fasteners. CEN, Brussels, Belgium.

38. EN 26891 (1991) Timber structures. Joints made with mechanical fasteners. General principles for the determination of strength and deformation characteristics CEN, Brussels, Belgium.

39. Muñoz W, Mohammad M, Salenikovich A, Quenneville P (2008) Need for a Harmonized Approach for Calculations of Ductility of Timber Assemblies. *41st CIB-W18 Meeting*, St. Andrews, Canada, Paper 41-15-1.

40. Muñoz W, Mohammad M, Salenikovich A, Quenneville P (2008) Determination of yield point and ductility of timber assemblies: in search for a harmonised approach. *World Conference on Timber Engineering (WCTE)*, Miyazaki, Japan.

41. EN 13183-1 (2002) Moisture content of a piece of sawn timber - Part 1 - Determination by oven dry method. CEN, Brussels, Belgium.

42. EN 384 (2010) Structural timber. Determination of characteristic values of mechanical properties and density. CEN, Brussels, Belgium.

Table 1. Mechanical properties of nails from tension tests and bending tests.

Property	Nail		
	μ	$COV[\mu]$	n
f_{u} [N/mm^2]	722.70	0.81%	5
M_{y} [Nmm]	6042.84	12.26%	10

Table 2. Characteristic strength capacities of nails from tension tests and bending tests, and comparison with calculation models.

Property	Nail
$f_{u,05}$ [N/mm^2]	639.04
$f_{u,95}$ [N/mm^2]	817.26
$M_{y,05}$ [Nmm]	4599.72
$M_{y,95}$ [Nmm]	7827.60
$M_{y,Rk\ B\&C}$ [Nmm]	5760.00
$M_{y,Rk\ EC5}$ [Nmm]	6616.50

Table 3. Mechanical properties of joints from nail withdrawal tests and physical properties of the CLT specimens used in the tests.

Property	Withdrawal ($n = 22$)	
	μ	$COV[\mu]$
K_{ser} [N/mm]	1283.01	23.52%
V_y [mm]	1.73	24.18%
F_y [N]	2018.13	15.05%
V_{max} [mm]	2.41	12.82%
F_{max} [N]	2148.66	14.76%
V_u [mm]	3.74	10.41%
F_u [N]	1718.45	14.75%
Duct [-]	2.27	23.82%
ρ [kg/m^3]	460.95	5.88%

Table 4. Characteristic strength capacities of joints from nail withdrawal tests and comparison with calculation models (with ρ_k = 410.85 kg/m3).

Property	Withdrawal
$F_{max,05}$ [N]	1604.94
$F_{max,95}$ [N]	2817.93
$F_{ax,Rk\ ETA}$ [N]	1437.99
$F_{ax,Rk\ ÖN}$ [N]	1415.20
$F_{ax,Rk\ B\&U}$ [N]	1458.22

Table 5. Mechanical properties of steel-to-timber joints from monotonic shear tests, in parallel and perpendicular direction to face lamination, and physical properties of the CLT specimens used in the tests.

Property	Shear			
	Parallel ($n=6$)		Perpendicular ($n=5$)	
	μ	$COV[\mu]$	μ	$COV[\mu]$
K_{ser} [N/mm]	483.69	17.81%	549.82	19.97%
V_y [mm]	7.63	27.67%	7.01	24.79%
F_y [N]	3508.51	5.39%	3916.14	9.66%
V_{max} [mm]	13.17	13.89%	12.90	9.83%
F_{max} [N]	3907.46	4.20%	4405.73	8.84%
V_u [mm]	22.66	27.23%	15.59	14.75%
F_u [N]	3275.26	4.32%	3877.99	12.06%
Duct [-]	3.13	37.95%	2.38	36.26%
ρ [kg/m^3]	477.44	1.46%	455.01	3.11%

Table 6. Mechanical properties of steel-to-timber joints from cyclic shear tests, in parallel and perpendicular direction to face lamination, and physical properties of the CLT specimens used in the tests.

Property	Shear			
	Parallel ($n = 15$)		Perpendicular ($n = 15$)	
	μ	$COV[\mu]$	μ	$COV[\mu]$
K_{ser} [N/mm]	545.55	32.04%	515.78	27.90%
V_y [mm]	6.66	26.50%	5.45	31.77%
F_y [N]	3393.21	14.80%	2735.23	11.06%
V_{max} [mm]	10.73	11.63%	8.62	23.97%
F_{max} [N]	3756.32	17.12%	3007.93	13.21%
$F_{max(3rd)}$ [N]	2411.62	14.88%	2268.71	9.49%
V_u [mm]	10.94	7.98%	9.94	24.98%
F_u [N]	3667.64	19.88%	2562.63	17.00%
$Duct$ [-]	1.75	25.87%	2.01	44.78%
$\nu_{eq(1st)}$ [%]	20.20%	16.94%	16.92%	10.82%
$\nu_{eq(3rd)}$ [%]	10.66%	17.77%	10.44%	13.82%
β_{Sd} [-]	0.71	7.73%	0.72	13.32%
ρ [kg/m^3]	472.66	4.35%	481.13	6.36%

Table 7. Characteristic strength capacities of steel-to-timber joints from monotonic shear tests and comparison with calculation models (with ρ_k = 422.14 kg/m3 for test series SH00 and ρ_k = 402.19 kg/m3 for test series SH90).

Property	Shear	
	Parallel	Perpendicular
$F_{max,05}$ [N]	3465.12	3549.46
$F_{max,95}$ [N]	4399.75	5435.40
$F_{v,Rk\ ETA}$ [N]	2674.63	2589.98
$F_{v,Rk\ EC5}$ [N]	2157.51	2097.29
$F_{v,Rk\ ÖN}$ [N]	2403.23	2403.23
$F_{v,Rk\ B\&U}$ [N]	2488.63	2421.38

 a.  b.

Figure 1. *Materials* - (a) Annular-ringed shank nails and (b) CLT elements used for withdrawal tests.


a.
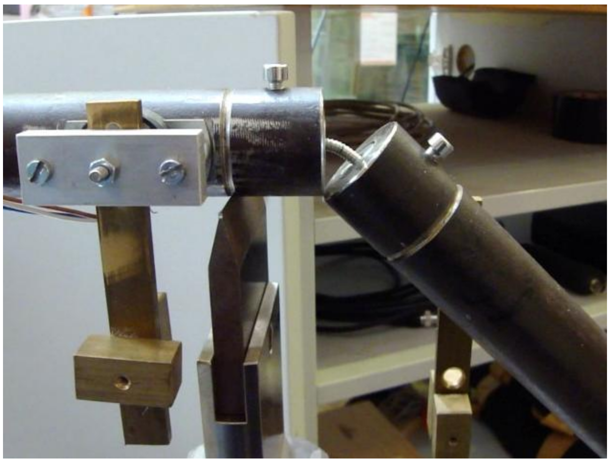
b.

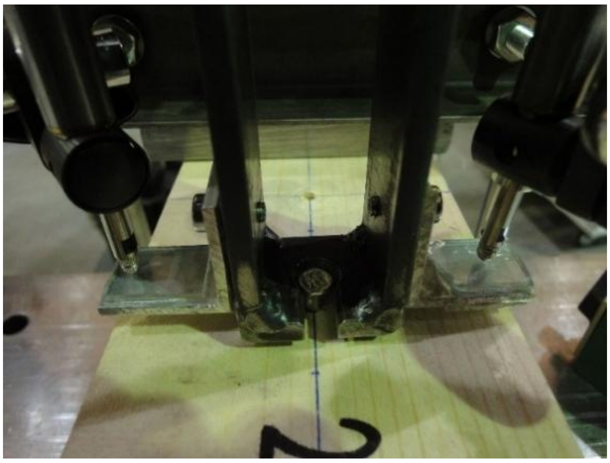
c.

d.

Figure 2. *Experimental setups* - (a) Tension tests, (b) bending tests, (c) nail withdrawal tests and (d) joint shear tests.

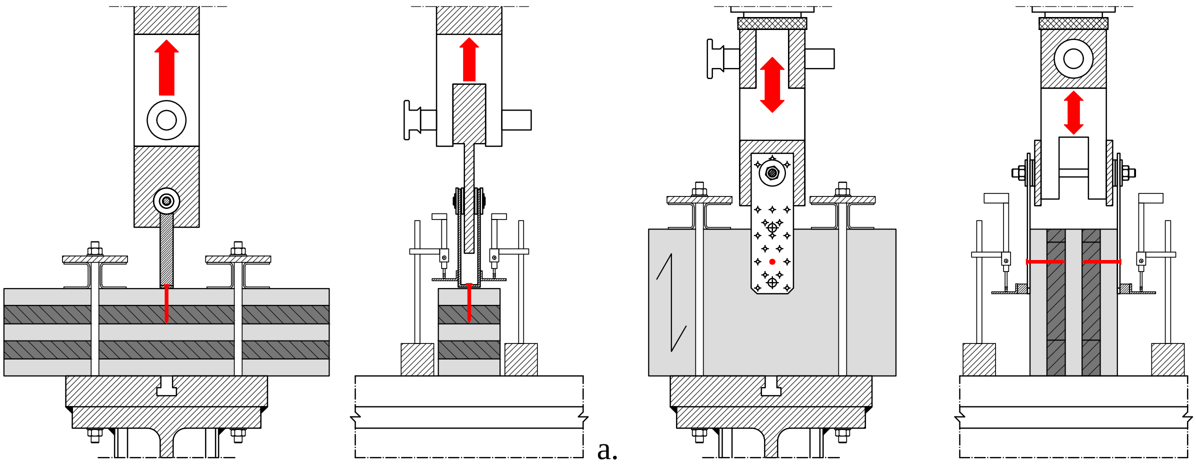

a. b.

Figure 3. *Test configurations for single fastener joint tests* - (a) Nail withdrawal tests (left: front view, right: side view) and (b) shear tests (left: front view, right: side view).

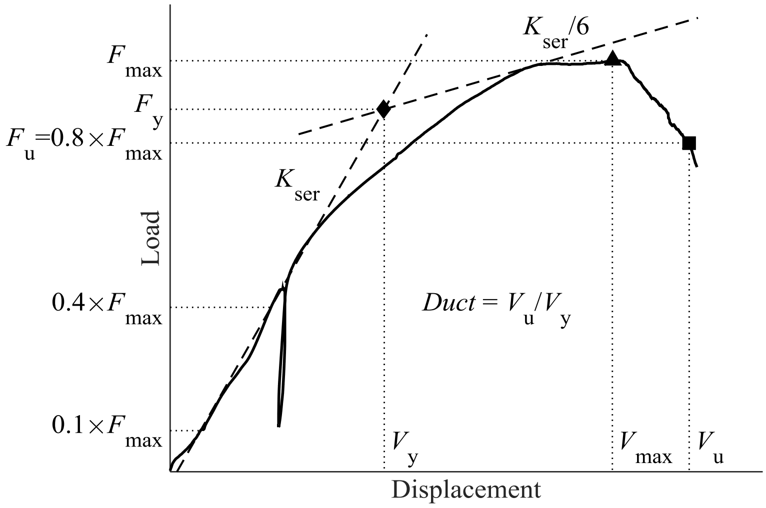

Figure 4. Model given in EN 12512:2001/A1 [18], used to evaluate the mechanical properties from the monotonic tests and from the first envelope curve of the cyclic tests.

 a. 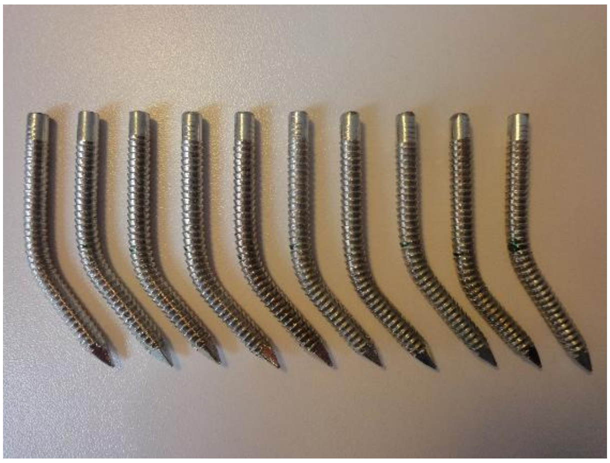 b.

Figure 5. (a) Failure modes of the tension tests and (b) deformed fasteners after bending tests.

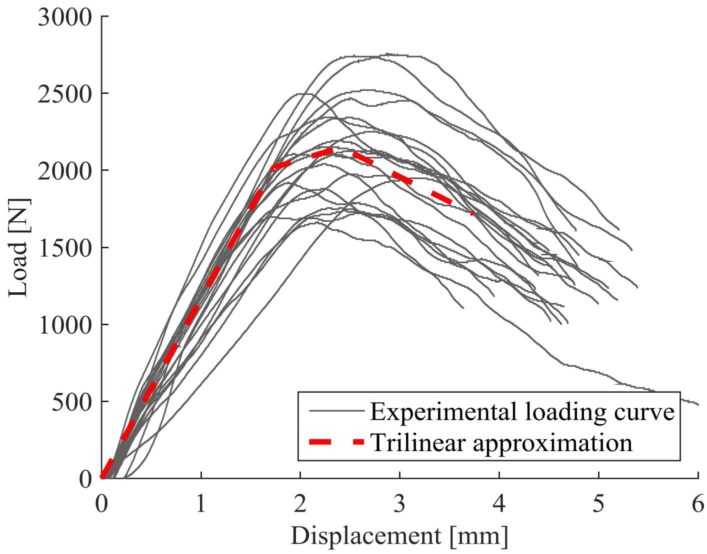

Figure 6. *Nail withdrawal tests* - Comparison among all the experimental results (grey solid lines) and trilinear approximating curve (red dashed line).

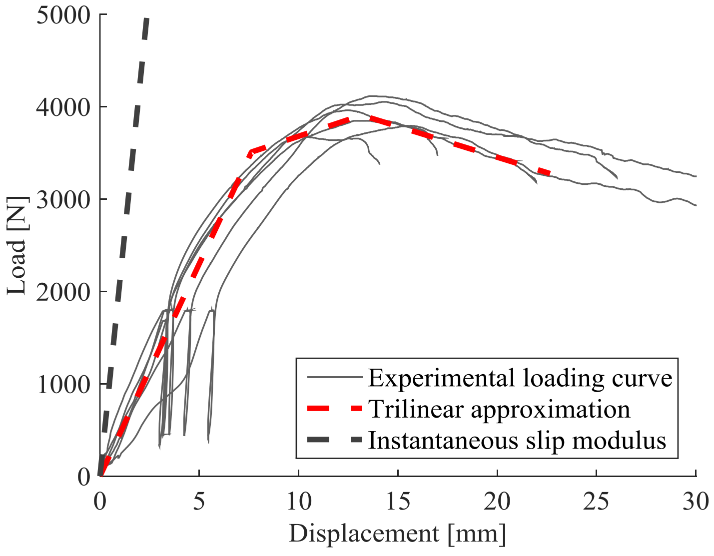

a.

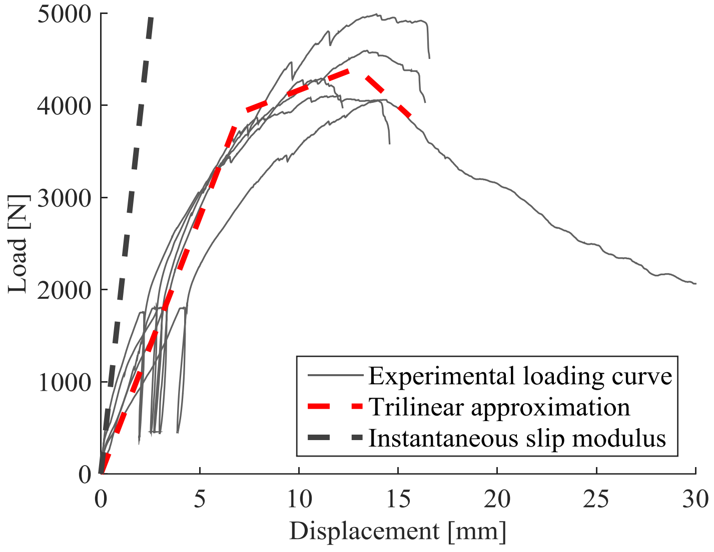

b.

Figure 7. *Monotonic shear tests* - Comparison among all the experimental results (grey solid lines), trilinear approximating curve (red dashed line) and instantaneous slip modulus (dark grey dashed line) according to Equation 16 (a) of specimens loaded in parallel to the face lamination of the CLT panel and (b) in perpendicular direction.

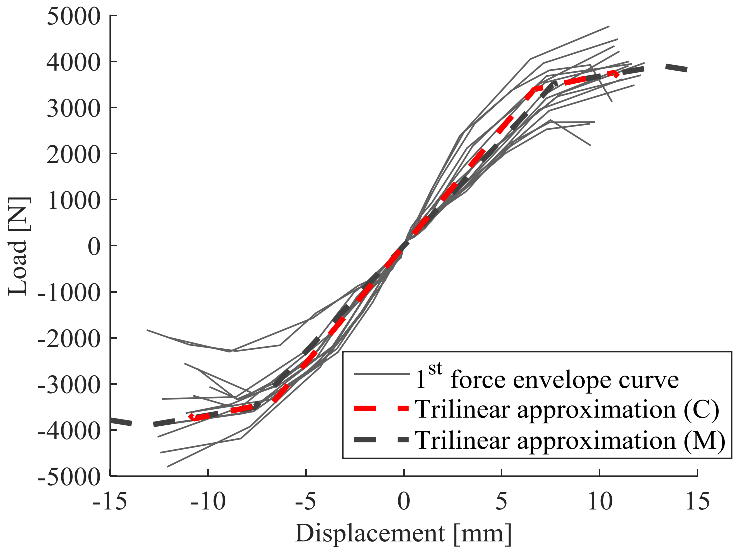

a.

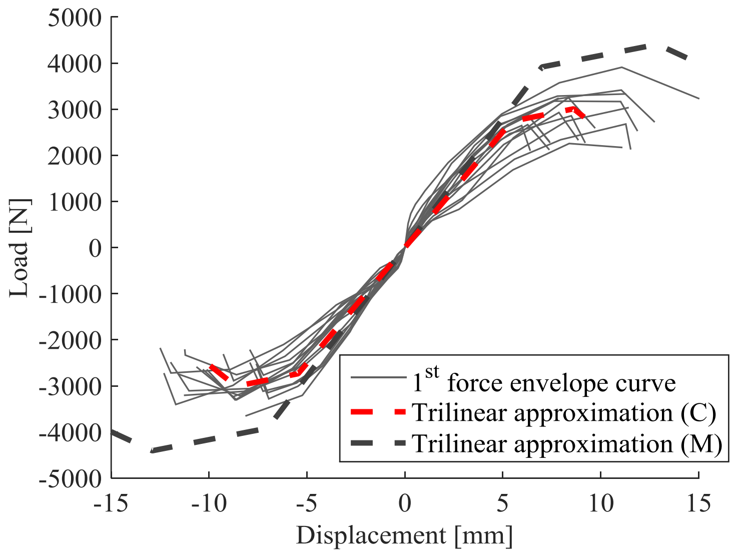

b.

Figure 8. *Cyclic shear tests* - Comparison among all the first envelope curves (grey solid lines), trilinear approximating curve determined from the cyclic tests (red dashed line) and from the monotonic tests (dark grey dashed line) (a) of specimens loaded in parallel to the face lamination of the CLT panel and (b) in perpendicular direction.

 a.  b.

Figure 9. *Single fastener joint shear tests* - Deformed fasteners (a) after monotonic tests and (b) after cyclic tests.